ACS APPLIED MATERIALS & INTERFACES

LETTER

www.acsami.org

Polymer/Polymer Blend Solar Cells with 2.0% Efficiency Developed by Thermal Purification of Nanoscale-Phase-Separated Morphology

Daisuke Mori,[†] Hiroaki Benten,[*,†] Junya Kosaka,[†] Hideo Ohkita,[†,‡] Shinzaburo Ito,[*,†] and Kunihito Miyake[§]

[†]Department of Polymer Chemistry, Graduate School of Engineering, Kyoto University, Katsura, Nishikyo, Kyoto 615-8510, Japan

[‡]PRESTO, Japan Science and Technology Agency (JST), 4-1-8 Honcho Kawaguchi, Saitama 332-0012, Japan

[§]Tsukuba Research Laboratory, Sumitomo Chemical Co., Ltd., 6 Kitahara, Tsukuba 300-3294, Japan

Supporting Information

ABSTRACT: We have fabricated polymer/polymer blend solar cells consisting of poly(3-hexylthiophene) as the electron donor and poly{2,7-(9,9-didodecylfluorene)-*alt*-5,5-[4′,7′-bis(2-thienyl)-2′,1′,3′-benzothiadiazole]} as the acceptor. The power conversion efficiency (PCE) was strongly dependent on solvents employed for spin coating. The best PCE of 2.0% was obtained for thermally annealed devices prepared from a chloroform solution, in contrast to devices fabricated from chlorobenzene and *o*-dichlorobenzene solutions. On the basis of the morphology−performance relationship in the polymer blends examined by atomic force microscopy and the photoluminescence quenching measurements, we conclude that the highly efficient performance is achieved by thermal purification of nanoscale-phase-separated domains formed by spin coating from chloroform.

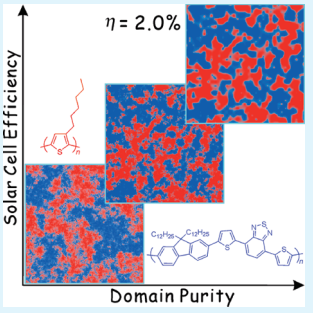

KEYWORDS: polymer photovoltaics, conjugated polymer blends, phase separation, morphology, poly(3-hexylthiophene), fluorene-based copolymer

Conjugated polymer-based solar cells are attracting attention as a possible inexpensive renewable energy source, owing to their advantages such as high throughput and large-area production by solution processes.[1] The photovoltaic layer of the most studied polymer-based solar cells is based on a blend of a conjugated polymer acting as an electron donor and a low-molecular-weight fullerene derivative, PCBM, as an acceptor.[2] On the other hand, polymer/polymer blend solar cells also have been a subject of active research[3,4] because they have potential advantages over polymer/fullerene blends such as more efficient light absorption due to acceptor polymers and relatively higher open-circuit voltages.[4] However, the power conversion efficiency (PCE) of polymer/polymer blend solar cells is still mostly lower than 2%,[4] which is far below that of polymer/fullerene solar cells.[2] The relatively poor efficiency has been considered to be due to the undesired morphology of blends such as a large phase separation,[5] inhomogeneous internal phase composition,[6−10] and reduced ordering of polymer chains.[11] The phase separation in polymer/polymer blends is probably different from that in polymer/fullerene blends.[12,13] It is therefore crucial to clarify how the blend morphology affects the device performance and how to obtain the optimal morphology that gives the best performance. In this letter, we demonstrate that the PCE of polymer/polymer blend solar cells consisting of poly(3-hexylthiophene) (P3HT) and poly{2,7-(9,9-didodecylfluorene)-*alt*-5,5-[4′,7′-bis(2-thienyl)-2′,1′,3′-benzothiadiazole]} (PF12TBT; Figure 1) is successfully improved up to 2.0% by optimizing the phase separation.

Figure 2 shows the *J*−*V* characteristics of P3HT/PF12TBT solar cells fabricated from *o*-dichlorobenzene (DCB), chlorobenzene (CB),

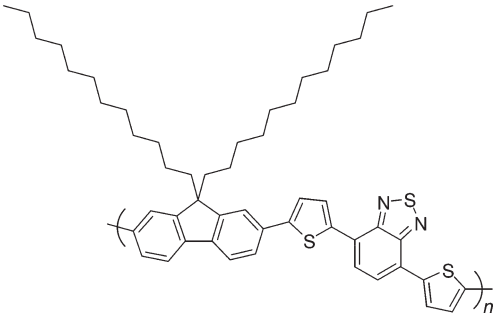

Figure 1. Chemical structure of PF12TBT.

and chloroform (CF) solutions with annealing at 140 °C for 10 min. The short-circuit current density (J_{SC}) was as low as 1 mA cm^{-2} for the devices from DCB and CB; these solvents are widely employed for polymer/fullerene solar cells to give a large J_{SC} and high PCE.[2] In contrast, a significant increase in J_{SC} up to 4 mA cm^{-2} was observed for the device from CF, and hence the PCE reached as high as 2.0%.[14] This is one of the best PCE values reported so far among polymer/polymer blend solar cells.[15−17] As shown in Figure 3a, the external quantum efficiency (EQE) of the device with a PCE of 2.0% was in good agreement in spectral shape with the UV−visible reflection absorption. This agreement suggests that both P3HT and PF12TBT equally contribute to the

Received: May 17, 2011
Accepted: June 29, 2011
Published: July 05, 2011

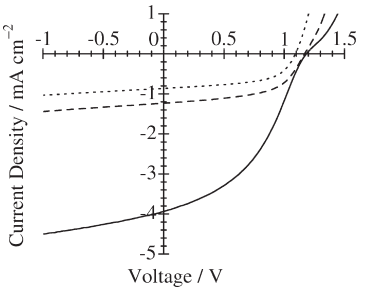

Figure 2. $J-V$ characteristics of P3HT/PF12TBT solar cells under AM 1.5G 100 mW cm^{-2} illumination. The devices were fabricated by spin coating from DCB (dotted line), CB (dashed line), and CF (solid line) solutions and annealed at 140 °C for 10 min. Device performances are summarized in Table 1.

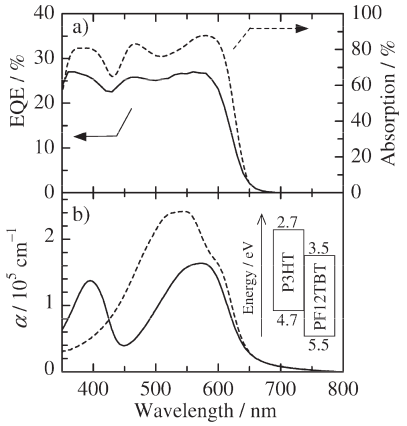

Figure 3. (a) EQE (solid line) and the UV−visible reflection absorption (dashed line) spectra of P3HT/PF12TBT solar cells with a PCE of 2.0%. (b) Absorption coefficients (α) of P3HT (dashed line) and PF12TBT (solid line) films. The inset shows the energy level diagram of P3HT and PF12TBT: the HOMO and LUMO levels were estimated by the photoelectron yield spectroscopy and the optical energy gap.

photocurrent generation. The EQE reached up to 27% at 560 nm and was still as high as 23% even at 600 nm, owing to the contribution of PF12TBT, which has an absorption peak around 575 nm (Figure 3b). The high EQE over 600 nm can account for the PCE being higher than that of another polymer/polymer blend solar cell based on P3HT and poly{2,7-(9,9-dioctylfluorene)-*alt*-5,5-[4′,7′-bis(4-hexyl-2-thienyl)-2′,1′,3′-benzothiadiazole]} (F8TBT; see Figures S1 and S3 in the Supporting Information), which is one of the most efficient polymer/polymer blend solar cells with a PCE of 1.8−1.9%.[16,17] Furthermore, the internal quantum efficiency (IQE) was higher than 30% (see Figure S4 in the Supporting Information). Such efficient photocurrent generation is partly due to energy offsets in the highest occupied molecular orbital (HOMO) and lowest unoccupied molecular orbital (LUMO) levels (0.8 eV) enough for charge separation, as shown in the inset in Figure 3b. We therefore conclude that the smaller optical band gap and larger absorption coefficient of PF12TBT than F8TBT (see Figure S5 in the Supporting Information) successfully lead to the significant increase in the PCE in the optimized device fabricated from CF. The efficient light absorption of PF12TBT might be due to the absence of hexyl chains at the 4 position of thiophene, which reduces the steric hindrance and increases the planarity of the polymer backbone.[18] The device parameters are summarized in Table 1.

Table 1. Device Performance and PL Quenching Efficiency

solvent	J_{SC} (mA cm^{-2})	V_{OC} (V)	FF	PCE (%)[a]	Φ_q (%)[b]
DCB	0.86	1.09	0.57	0.54	45 ± 4
CB	1.23	1.17	0.56	0.80	50 ± 4
CF	3.94	1.19	0.42	2.0	71 ± 4

[a] More than six devices were fabricated. The highest PCE and average values were 0.58% and 0.54% for DCB, 0.82% and 0.78% for CB, and 2.12% and 1.97% for CF, respectively. [b] PL quenching efficiency of PF12TBT.

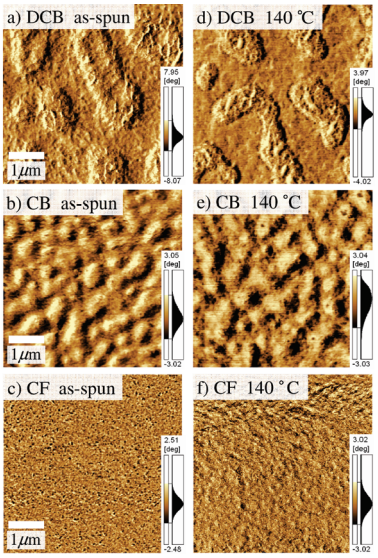

Figure 4. Tapping-mode AFM phase images (5 μm × 5 μm) of P3HT/PF12TBT blend films spin-coated from (a and d) DCB, (b and e) CB, and (c and f) CF solutions on glass substrates: (a−c) as-spun films; (d−f) annealed films at 140 °C for 10 min. The scale bar corresponds to a length of 1 μm.

To address the origin of the different device performances depending on the spin-coating solvents, we measured atomic force microscopy (AFM) phase images of P3HT/PF12TBT blend films before and after thermal annealing. As shown in Figure 4a−c, marked differences were observed for the three blend films fabricated from different solutions before thermal annealing. For the blend film spin-coated from DCB, phase-separated structures were clearly observed: each domain was a few micrometers in lateral dimension (Figure 4a). For the blend film from CB, smaller but still distinct phase-separated structures were observed: each domain was a few hundred nanometers in lateral dimension (Figure 4b). In either case, the phase-separated domains are much larger than the exciton diffusion length of typical conjugated polymers (≤10 nm).[19] In contrast, no distinct phase-separated structures were observed for the blend film from CF, suggesting a well-mixed blend morphology of P3HT and PF12TBT (Figure 4c). More importantly, as shown in Figure 4d−f, no distinct change in the phase-separated structures was observed for all of the blend films before and after thermal annealing. Even at 200 °C for 10 min, thermal annealing caused little change in the surface morphology (see Figure S6 in the Supporting Information). We therefore conclude that large-scaled

phase-separated structures are less sensitive to thermal annealing but rather are primarily dependent on the spin-coating solvent. The spontaneous large phase separation during spin coating from DCB and CB solutions is one of the reasons that limits the efficiency of the devices.

We next measured the photoluminescence (PL) quenching efficiency Φ_q of PF12TBT in the P3HT/PF12TBT blend films before and after thermal annealing. Before thermal annealing, Φ_q reached to 89% for CF and was as high as 60% even for DCB and CB. The high Φ_q for CF is consistent with well-mixed blend structures observed in the AFM image (Figure 4c). In contrast, the high Φ_q observed for DCB and CB is apparently inconsistent with large phase-separated structures on a scale of micro- or submicrometers, as shown in Figure 4a,b. Such a disagreement has been reported for blends of conjugated polymers, suggesting that large phase-separated domains are not pure but involve a minor counterpart material.[3,5−9] The minor counterpart isolated in the large domains just serves as a quenching site for excitons but cannot contribute to photocurrent generation because, even if charge carriers can be generated from excitons, the minor counterpart cannot transport a carrier to an electrode. This is consistent with the small J_{SC} observed for DCB and CB. Therefore, it can be said that spontaneous large phase separation and undesired exciton quenching by the minor counterpart lead to small J_{SC} and thus low PCE of the devices fabricated from DCB and CB. Interestingly, Φ_q for all of the blend films decreased after thermal annealing: 71% for CF, 50% for CB, and 45% for DCB. This is again inconsistent with phase-separated structures observed in the AFM images: no change was observed before and after thermal annealing. We therefore conclude that thermal annealing does not affect large-scaled phase-separated structures but rather induces phase separation on a nanometer scale.

Finally, we focus on the efficient device fabricated from CF to discuss the relationship between the device performance and the blend morphology in detail on the basis of the dependence of the device parameters and Φ_q on the annealing temperature. As shown in Figure 5a, with increasing annealing temperature, J_{SC} increased from 1.1 mA cm^{-2} for the as-spun device to 4.2 mA cm^{-2} for the device annealed at 120 °C and then decreased above it. The fill factor (FF) increased from 0.23 for the as-spun device to 0.45 for the device annealed at 160 °C and then decreased slightly. The open-circuit voltage (V_{OC}) was kept constant at around 1.1−1.2 V independently of the temperature (Figure 5b). Such an annealing temperature dependence of J_{SC}, FF, and V_{OC} indicates that the maximum PCE at 140 °C results from the balance between J_{SC} and FF (Figure 5c). On the other hand, Φ_q was as high as ∼90% for the as-spun film and the annealed films at 80 and 100 °C, but with increasing annealing temperature, it monotonically decreased and finally was 32% at 200 °C (Figure 5b). To elucidate how the nanoscale phase separation impacts the performance, J_{SC} was replotted against Φ_q in Figure 5d. As shown in Figure 5d, J_{SC} steeply increases from 1.1 mA cm^{-2} for the as-spun device to 3.9 mA cm^{-2} for the annealed device at 100 °C even though Φ_q remains as high as ∼90%. In contrast, J_{SC} decreases from 4.2 to 2.0 mA cm^{-2} in proportion to Φ_q for devices annealed above 120 °C. Thermal annealing should increase the domain purity or domain size. The improvement in the domain purity results in an increase in J_{SC} because undesirable exciton quenching is reduced and carrier transport would be improved. The growth in the domain size causes a decrease in the domain interface and hence in J_{SC}. Thus, an increase in J_{SC} below 100 °C is indicative of an increase in the domain purity, and a decrease in J_{SC} above 120 °C is ascribable

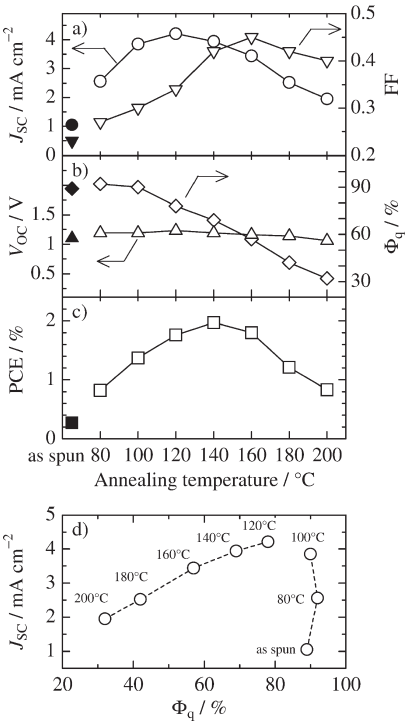

Figure 5. Dependence of the device parameters and Φ_q on the annealing temperature: (a) J_{SC} (open circles) and FF (open inverted triangles), (b) V_{OC} (open triangles) and Φ_q (open diamonds), and (c) PCE (open squares). The closed symbols represent the device parameters and Φ_q before thermal annealing. (d) Plots of J_{SC} against their respective Φ_q. These parameters were measured for P3HT/PF12TBT solar cells fabricated by spin coating from CF.

to an increase in the domain size. A recent Monte Carlo simulation has demonstrated that, under the condition of each domain size being less than 80 nm, the domain purity should be more than 95% to account for $\Phi_q \approx 90\%$ and almost 100% for $\Phi_q \approx 30\%$.[20] We therefore conclude that thermal annealing below 100 °C mainly improves the purity of small domains, and above 120 °C, it further induces the growth of the highly pure domain in size on a nanometer scale.

In summary, we find that phase-separated structures on a scale of micro- or submicrometers are less sensitive to thermal annealing but rather are primarily dependent on the spin-coating solvent and that thermal annealing rather induces phase separation on a nanometer scale. On the basis of these findings, we fabricate highly efficient polymer/polymer blend solar cells by spin coating from CF with thermal annealing. The low-boiling solvent of CF gives a well-mixed blend morphology consisting of nanoscale-phase-separated domains. Thermal annealing improves the domain purity at low temperatures and promotes the growth of the domain size on a nanometer scale at high temperatures. The best PCE of 2.0% is achieved with an optimum phase-separated structure, which cannot be obtained from DCB and CB solutions because of the micrometer-scaled phase-separated structures with a minority counterpart.

EXPERIMENTAL SECTION

Photovoltaic devices were fabricated by spin coating from a blend solution of P3HT (Aldrich; M_w = 87 000, regioregularity >90%) and PF12TBT (Sumitomo Chemical Co., Ltd.; M_w = 20,000,

M_w/M_n = 2.0, T_g = 76 °C) onto an indium−tin oxide (ITO) substrate with a 40-nm-thick topcoat layer of poly(3,4-ethylenedioxythiophene):poly(4-stylenesulfonate) (PEDOT:PSS; H.C. Stark PH-500). The blend solution was prepared by mixing P3HT and PF12TBT with a weight ratio of 1:1 in DCB, CB, and CF. The thickness of the P3HT/PF12TBT blend layer was approximately 70 nm. The photoactive layer was thermally annealed for 10 min in a N_2-filled glovebox after vacuum deposition of a lithium fluoride (LiF, 1 nm) and aluminum electrode (Al, 70 nm). The $J-V$ characteristics of the devices were measured in a N_2 atmosphere under AM1.5G simulated solar light at 100 mW cm^{-2}. The absolute reflectivity was measured for the device samples at an incident angle of 5° normal to the substrate (Hitachi U-4100). The light was irradiated from the ITO side. The AFM images were collected in tapping mode (Shimadzu SPM-9600) using silicon probes with a tip radius typically smaller than 8 nm. The PL quenching efficiency of PF12TBT was evaluated from the ratio of the PL intensity excited at 392 nm for P3HT/PF12TBT blend films to that for a PF12TBT neat film, spin-coated on glass substrates. The HOMO level of a P3HT and PF12TBT neat film was estimated by photoelectron yield spectroscopy (AC-3, Riken Keiki).

■ ASSOCIATED CONTENT

Supporting Information. Device fabrication and characterization methods, comparison of EQE spectra between P3HT/PF12TBT and P3HT/F8TBT solar cells, IQE spectrum of a P3HT/PF12TBT solar cell, absorption coefficients of PF12TBT and F8TBT, and AFM topographic image of a P3HT/PF12TBT blend film annealed at 200 °C. This material is available free of charge via the Internet at http://pubs.acs.org.

■ AUTHOR INFORMATION

Corresponding Author

*Tel.: +81 75 383 2614 (H.B.), +81 75 383 2612 (S.I.). Fax: +81 75 383 2617 (H.B.), +81 75 383 2617 (S.I.). E-mail: benten@photo.polym.kyoto-u.ac.jp (H.B.), sito@photo.polym.kyoto-u.ac.jp (S.I.).

■ ACKNOWLEDGMENT

This work was supported by a FIRST Program and a Grant-in-Aid for Young Scientists (B) (22750109) from JSPS, a PRESTO program from JST, and a Global COE program from MEXT.

■ REFERENCES

(1) Krebs, F. C.; Tromholt, T.; Jørgensen, M. *Nanoscale* **2010**, *2*, 873–886.
(2) Dennler, G.; Scharber, M. C.; Brabec, C. J. *Adv. Mater.* **2009**, *21*, 1323–1338.
(3) Veenstra, S. C.; Loos, J.; Kroon, J. M. *Prog. Photovoltaics: Res. Appl.* **2007**, *15*, 727–740.
(4) McNeill, C. R.; Greenham, N. C. *Adv. Mater.* **2009**, *21*, 3840–3850.
(5) Arias, A. C.; MacKenzie, J. D.; Stevenson, R.; Halls, J. J. M.; Inbasekaran, M.; Woo, E. P.; Richards, D.; Friend, R. H. *Maclomolecules* **2001**, *34*, 6005–6013.
(6) Snaith, H. J.; Arias, A. C.; Morteani, A. C.; Silva, C.; Friend, R. H. *Nano Lett.* **2002**, *2*, 1353–1357.
(7) Shikler, R.; Chiesa, M.; Friend, R. H. *Macromolecules* **2006**, *39*, 5393–5399.
(8) McNeill, C. R.; Watts, B.; Thomsen, L.; Belcher, W. J.; Greenham, N. C.; Dastoor, P. C.; Ade, H. *Macromolecules* **2009**, *42*, 3347–3352.
(9) Swaraj, S.; Wang, C.; Yan, H.; Watts, B.; Lüning, J.; McNeill, C. R.; Ade, H. *Nano Lett.* **2010**, *10*, 2863–2869.
(10) Moore, J. R.; Albert-Seifried, S.; Rao, A.; Massip, S.; Watts, B.; Morgan, D. J.; Friend, R. H.; McNeill, C. R.; Sirringhaus, H. *Adv. Energy Mater.* **2011**, *1*, 230–240.
(11) McNeill, C. R.; Abrusci, A.; Hwang, I.; Ruderer, M. A.; Müller-Buschbaum, P.; Greenham, N. C. *Adv. Funct. Mater.* **2009**, *19*, 3103–3111.
(12) Nilsson, S.; Bernasik, A.; Budkowski, A.; Moons, E. *Macromolecules* **2007**, *40*, 8291–8301.
(13) Müller, C.; Ferenczi, T. A. M.; Campoy-Quiles, M.; Frost, J. M.; Bradley, D. D. C.; Smith, P.; Stingelin-Stutzmann, N.; Nelson, J. *Adv. Mater.* **2008**, *20*, 3510–3515.
(14) An inflection point near V_{OC} in the $J-V$ curve measured for the device from CF would be caused by the unoptimized thickness of the LiF layer. The slightly thick LiF layer may have a negative impact on the charge collection from the polymer blend to the aluminum electrode.
(15) Zhou, E.; Cong, J.; Wei, Q.; Tajima, K.; Yang, C.; Hashimoto, K. *Angew. Chem., Int. Ed.* **2011**, *50*, 2799–2803.
(16) McNeill, C. R.; Abrusci, A.; Zaumseil, J.; Wilson, R.; McKiernan, M. J.; Burroughes, J. H.; Halls, J. J. M.; Greenham, N. C.; Friend, R. H. *Appl. Phys. Lett.* **2007**, *90*, 193506.
(17) He, X.; Gao, F.; Tu, G.; Hasko, D.; Hüttner, S.; Steiner, U.; Greenham, N. C.; Friend, R. H.; Huck, W. T. S. *Nano Lett.* **2010**, *10*, 1302–1307.
(18) Li, W.; Qin, R.; Zhou, Y.; Andersson, M.; Li, F.; Zhang, C.; Li, B.; Liu, Z.; Bo, Z.; Zhang, F. *Polymer* **2010**, *51*, 3031–3038.
(19) Markov, D. E.; Amsterdam, E.; Blom, P. W. M.; Sieval, A. B.; Hummelen, J. C. *J. Phys. Chem. A* **2005**, *109*, 5266–5274.
(20) McNeill, C. R.; Westenhoff, S.; Groves, C.; Friend, R. H.; Greenham, N. C. *J. Phys. Chem. C* **2007**, *111*, 19153–19160.